International Symposium
On Turbulence and Shear Flow
Phenomena (TSFP-8)
August 28 - 30, 2013 Poitiers, France

EFFECT OF TURBULENT TO LAMINAR FLOW TRANSITION ON SURFACE REACTION AND PARTICLE DEPOSITION IN A SQUARE DUCT

Kenji Tanno, Hisao Makino
Energy Engineering Research Laboratory
Central Research Institute of Electric Power Industry
2-6-1 Nagasaka, Yokosuka, Kanagawa, 240-0196, Japan
k-tanno@criepi.denken.or.jp, makino@criepi.denken.or.jp

Ryoichi Kurose, Satoru Komori
Department of Mechanical Engineering and Science
Kyoto University
Kyoto daigaku-Katsura, Nishikyo-ku, Kyoto, 615-8140, Japan
kurose@mech.kyoto-u.ac.jp, komori@mech.kyoto-u.ac.jp

Takenobu Michioka
Environmental Science Research Laboratory
Central Reseach Institute of Electric Power Industry
1646 Abiko, Abiko, Chiba, 270-1194, Japan
michioka@criepi.denken.or.jp

ABSTRACT

A monolith reactor is widely used to reduce pollutant matter in the industrial field. A monolith reactor, which consist of many rectangular channels, although flue gas flows into the channel inlet in turbulent condition, flue gas transitions from turbulent to laminar flow due to the small hydraulic diameter of a single channel. In order to develop a higher performance reactor, optimize the maintenance schedule and extend lifetime of reactor, it is important to understand reaction and degradation mechanism in a monolith reactor. In this study, surface reaction behaviour occurred on the wall and particle adhesion behaviour is investigated performing a direct numerical simulation (DNS). The results show that both surface reaction and particle adhesion are promoted by turbulent eddies which exists in the upstream region. However, the region which exhibits the effect of turbulent eddies is different. For particle deposition, the effect of turbulent eddies exhibits only in the upstream region, whereas for surface reaction, such effect also exhibits in the downstream region. This is because of the remaining cross-sectional fluid motion caused by the inflow turbulence. The magnitude of the cross-sectional fluid motion is weak, hence such motion only affects gaseous flow and cannot affect heavy particle motion.

INTRODUCTION

A catalytic monolith reactor is widely used to reduce pollutant matter both in a car and a thermal power plant. A monolith reactor consists of a large number of parallel channels separated by thin wall. The channel usually has a small hydraulic diameter, hence the Reynolds number in a single channel is does lie in the range of laminar flow for the most of actual operation condition. However, the upstream channel in the monolith reactor is usually far larger than the size of a single channel of the monolith reactor, so that the upstream flue gas flow in the inlet of monolith reactor is usually turbulent. Therefore, the inner flow is supposed to transition from turbulent to laminar flow downstream in the reactor.

Such flow transition should affect surface reaction in the monolith reactor (ex. catalytic de-NO_x reaction). Kinetic and modelling studies of surface reaction in the monolith reactor have been investigated by using one-dimensional plug-flow reactor models (Beeckman and Hegedus ,1991; Roduit et al., 1998; Tronconi and Beretta, 1999; Forzatti, 2001) and three dimensional monolith models (Hays and Kolaczkowski, 1994; Fogler, 2005; Ström and Sasic, 2012). However, since turbulent-laminar flow transition is difficult to account for, these effects have been neglected in previous studies.

In honeycomb reactor, flue gas is often particle-laden flow, and particle deposition to the wall sometimes affects reactor efficiency, for example, ash particle deposits reactor surface in the de-NOx equipment in a thermal power plant and coverage of ash particle degrades the performance of the equipment. Therefore, it is also important to investigate the particle deposition behavior in a monolith reactor.

Extensive literature exists on particle-laden turbulent flows that have two homogeneous directions, such as isotropic turbulence, channels and circular pipes. However, considerably less work exits on the particle-

laden flow in the square duct. Phares and Sharma (2006) investigated small particle deposition behavior in a turbulent square duct using a direct numerical simulation and clarified the effect of secondary flow on the particle motion and particle deposition. Winkler and Rani (2009) investigated the particle forces in a turbulent square duct using large eddy simulation. However, they adopted the fully developed turbulent flow, and particle deposition behavior in the turbulent to laminar transition flow is never investigated.

Therefore, the purpose of this study is to investigate the surface reaction and particle deposition behavior in the turbulent-laminar transition flow in a square duct using a direct numerical simulation coupled with Lagrangian particle tracking. The surface reactions are assumed to take place in the computational cell closest to the wall and reaction rate is given by a Langmuir-Hinshelwood-type rate expression. A particle is assumed to deposit when it reaches a distance from the wall equal or less than its radius.

NUMERICAL METHOD

Governing Equations for Continuous Phase

The governing equations for reactive turbulent flow are continuity, momentum (the Navier-Stokes equaton) and mass conservation equations for species i are written as

$$\frac{\partial U_i}{\partial x_i} = 0 \tag{1}$$

$$\frac{\partial U_i}{\partial t} + \frac{\partial U_j U_i}{\partial x_j} = -\frac{\partial P}{\partial x_i} + \frac{1}{\mathrm{Re}}\frac{\partial^2 U_i}{\partial x_j \partial x_j} + \Psi_{u_i} \tag{2}$$

$$\frac{\partial \Gamma_i}{\partial t} + \frac{\partial U_j \Gamma_i}{\partial x_j} = \frac{1}{ReSc}\frac{\partial^2 \Gamma_i}{\partial x_j \partial x_j} + \omega \tag{3}$$

where U_i and Γ_i and P are respectively the instantaneous i component velocity, instantaneous concentration of chemical species i and instantaneous pressure. Ψ_{ui} in eq.(2) is the momentum exchange between the continuous and dispersed phase, which is considered by the particle-source-in-cell (PSI-Cell) method (Crowe et al.,1977) and is expressed as

$$\Psi_{u_i} = -\frac{1}{\delta_c}\sum^{n_c}\frac{m_p \Phi}{\tau_p}\left(U_i - U_{p,i}\right) \tag{4}$$

where $U_{p,i}$ is the particle velocity of particle number i, δ_c is the cell volume ($\delta_c = \Delta_1\Delta_2\Delta_3$, Δ_i is the width of the computational grid) and n_c is the number of solid particle within the volume of the grid. Φ is shown later. In eq. (3), ω is a chemical reaction source term, described in detail below. These equations are normalized using the channel width L=0.006m, inlet bulk velocity U_b=6m/s, kinematic viscosity $\nu = 5.67\times10^{-5}\mathrm{m^2s^{-1}}$ and initial NO concentration Γ_{NO}=300ppm. These value are set to match the actual de-NO_x equipment operation condition in thermal power plants. The Reynolds number, Re and Schmidt number, Sc, are defined as

$$Re = \frac{U_b L}{\nu} \tag{5}$$

$$Sc = \frac{\nu}{D} \tag{6}$$

where D is the molecular diffusivity of NO in air and Sc is set to 1.0 for exhaust flow.

Governing Equations for Dispersed Phase

The solid particles are tracked individually in a Lagrangian manner. It is assumed that the particle material density is much larger than the fluid density, $\rho_p \gg \rho_f$, such that the dominating forces acting on the particle by the surrounding fluid are the drag and other forces (the lift, pressure gradient, added mass and Basset) can be neglected. Furthermore, the gravity force is also neglected.

The non-dimensional Lagrangian particle equations are given as

$$\frac{dx_{p,i}}{dt} = U_{p,i} \tag{7}$$

$$\frac{dU_{p,i}}{dt} = -\frac{1}{\tau_p}\left(U_{p,i} - U_i\right)\Phi \tag{8}$$

where τ_p is referred to as the particle response time, which is defined by

$$\tau_p = \frac{d_p^2 \rho_p Re}{18\mu} \tag{9}$$

where Φ (Glaze and Frankel, 2000) is given as

$$\Phi = \begin{cases} 1 + \frac{3}{16}Re_p & \left(Re_p \le 0.01\right) \\ 1 + 0.1315 Re_p^{(0.82-0.05w)} & \left(0.01 \le Re_p \le 20\right) \end{cases} \tag{10}$$

with

$$w = \log_{10} Re_p \tag{11}$$

Here, Rep is the particle Reynolds number based on the particle diameter, dp, and the relative velocity between the particle and fluid:

$$Re_p = \frac{d_p \left|U_{p,i} - U_i\right| \rho_f}{\mu} \tag{12}$$

De-NO_x Reaction on the Wall Surface

The de-NO_x reaction is assumed to occur only in the computational cell closest to the wall. Reaction rate is given by the Langmuir-Hinshelwood type rate expression as (Beeckmann and Hegedus, 1991)

$$\omega = Sk_0 \exp\left(-\frac{E}{RT}\right)\Gamma_{NO}\left[\frac{K_{NH_3}\Gamma_{NH_3}}{1 + K_{NH_3}\Gamma_{NH_3}}\right] \tag{7}$$

where S, k_0, E, R, T, ΓNO, Γ_{NH3} and K_{NH3} are respectively the specific surface area, pre-exponential factor, activation energy, gas constant (=8.314JK^{-1}mol^{-1}), gaseous temperature, NO and NH_3 concentration and NH_3 adsorption constant.

Computational Details

Figure 1 shows a schematic diagram of the de-NO_x equipment in a thermal power plant, catalyst element and the computational domain. The computational domain represents the upstream region of a single square duct channel in a honeycomb reactor. The dimension-less computational domain was 10.0 × 1.0× 1.0 in the streamwise (x), vertical (y) and spanwise (z) directions. The origin of the co-ordinate axes, x, y and z was set at the center of the inlet y-z plane. Non-slip boundary conditions were imposed on the velocity component on the upper, lower and side walls. Neumann boundary condition ($\partial\Gamma/\partial x_n$=0) was imposed on the scalar component. Convective boundary conditions ($\partial U_i/\partial t+ \overline{U}\ \partial U_i/\partial x$=0) were applied at the exit of teh domain. These boundary conditions avoid the problem caused by pressure perturbations being reflected off the outflow boundary back to the computational domain (Ferziger and Peric, 2002).

In this study, the calculations were performed for a laminar inflow condition and a turbulent inflow condition in order to investigate the effects of inflow behaviour. For laminar inflow case, the fluid is uniformly flows into the computational domain. On the other hand, in order to simulate a turbulent inflow condition, three-dimensional isotropic turbulence was generated by the spectrum method (Michioka, 2001) prior to the main DNS calculation; the resulting flow profiles were stored and imposed on the domain inlet at each time step.

The governing equations of eq. (1)-(3) were discretized on a staggered mesh arrangement to construct a fully consistent and conservative finite-difference formation. The spatial derivatives in these equations were approximated by a forth-order central difference scheme except for the convection term in the mass-conserved equation. A flux-transport (FCT) scheme (Boris and Book, 1973; Book et al. 1975; Boris and Book, 1976; Michioka et al., 2003) was applied to this term, since the second- or fourth order central difference scheme may produce a negative value. The fractional step method (Kim and Moin, 1985) was used to solve the N-S equation. The time integration of eq. (2) and (3) was carried out using a third-order low-storage Runge-Kutta method (Williamson, 1980). The numbers of the DNS grid points were 400 × 128 × 128 in the streamwise, vertical and spanwise directions, respectively. In order to correctly simulate the near-wall regions, a non-uniform grid with a hyperbolic tangent stretching (Huser, 2003) was used in the y and z directions. To implement the DNS, the computational grid size must be smaller than the smallest turbulent length scale (Kolmogorov scale) and the smallest concentration scale (Bachler scale). In this present DNS, the Bachelor scale is equal to Kolmogorov scale because Sc = 1. The largest grid size was set to be smaller than these scales,

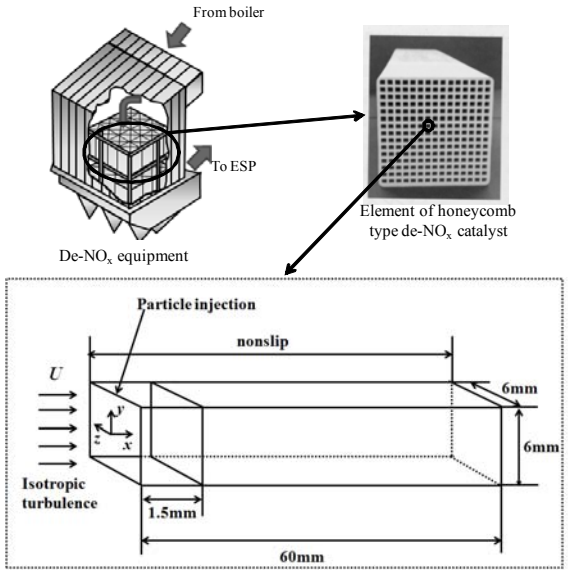

Figure 1. Schematic of diagram of the de-NOx equipment in a thermal power plant, catalyst element and the computational domain.

Which were estimated in the inlet turbulence in the turbulent inflow case. The time step, Δt, was set to 2.0 × 10^{-4} s.

In this study, injected particles represent fly ash, hence particle density, ρ_p, and particle diameter, d_p, are set to 2200kg/m^3 and 15μm, respectively. The flow was assumed to be dilute; hence no particle-particle interaction was taken into account. Particles are injected from the inlet of computational domain and injection rate was set to 2.6. × 10^5 number/s. The initial velocities of the particles are set equal to the interpolated fluid velocities at each particle location. The time-integration of eq. (8) is carried out using a second-order Adams-Bashforth method with the same time step as the continuous phase. It is assumed that all of particles, which reaches a distance from the wall equal or less than its radius, deposit on the wall.

RESULTS AND DISCUSSION

Flow Behavior in a Monolith Reactor

Figure 2 shows the instantaneous and time averaged streamwise and time-averaged streamwise velocities on the (x, y) plane at z=0.It is clearly seen that inner flow, which is uniformly injected to the channel, gradually develops a laminar boundary layer in the laminar inflow case, whereas the flow patterns are complex near the inlet and flow transitions from turbulent to laminar flow in the turbulent inflow case. Turbulence flow structure is often characterized by the second invariant of the velocity gradient tensor ∇u. The instantaneous iso-surfaces of the second invariant Q = 1.0 for the turbulent inflow case are shown in figure 3. Just downstream of the inlet, narrow tube-like structure can be seen. This vortex shape is typical of the isotropic turbulence. However, clusters glow large and hairpin-like structure appears near the wall. It is suspected that these hairpin-like vortices appear due to the strong skin friction near the wall. These vortices then

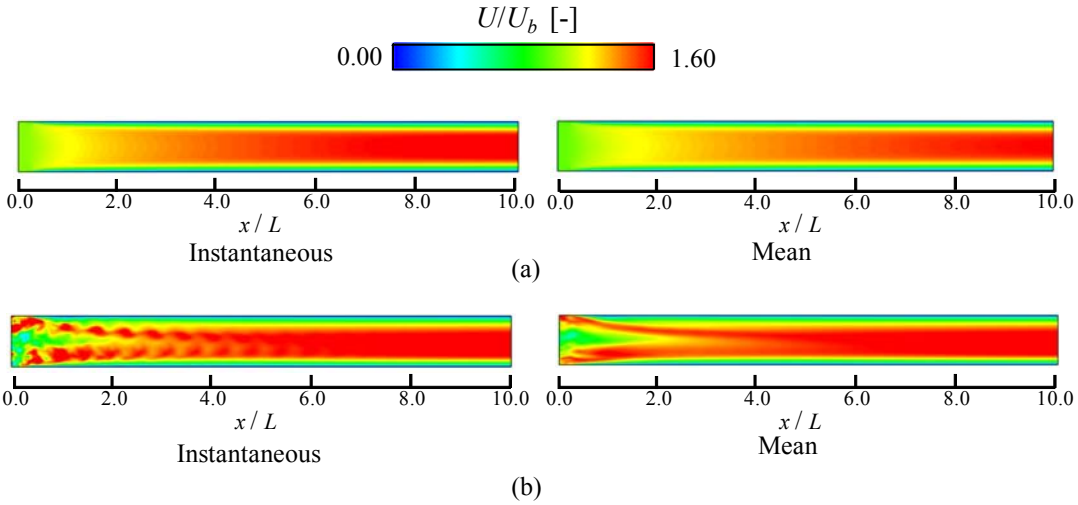

Figure 2. Instantaneous and time averaged distributions of streamwise velocity on the plane of z=0: (a) laminar inflow case; (b) turbulent inflow case.

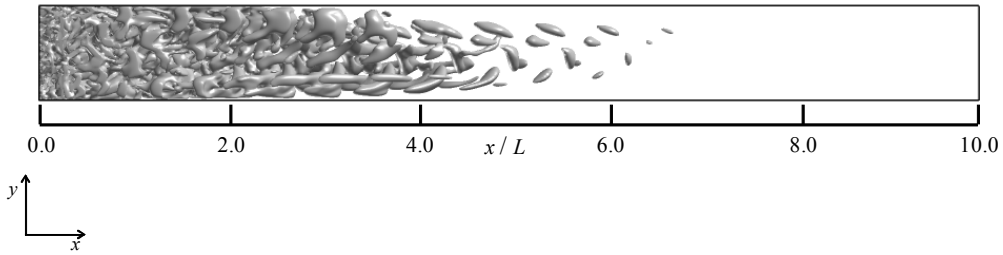

Figure 3. Visualization of turbulent structures through the second invariant of the velocity gradient tensor Q = 1.0 for turbulent inflow condition.

disappear in the downstream region due to the fluid viscosity.

Surface Reaction Behavior

Figure 4 shows the instantaneous and time-averaged NO concentration in the (x, y)-plane at z=0. The development of a concentration boundary layer towards downstream can be seen for both cases. In the instantaneous distribution, the NO concentration is disturbed by turbulence for the turbulent inflow condition. In the time-averaged distributions, on the other hand, no significant difference can be seen between laminar and turbulent inflow case, unlike the case with the instantaneous distributions.

In order to quantify the effects of turbulence on the surface reaction, we calculated the reaction efficiency, E_r, defined as $E_r=(\Gamma_{NO,0} - \Gamma_{NO,x}) / \Gamma_{NO,0}$. Here, $\Gamma_{NO,0}$ is the initial NO concentration and $\Gamma_{NO,x}$ is the cross-sectional-averaged NO concentration. Therefore, E_r of 1 means that NO is completely decomposed. Figure 5 shows the streamwise distributions of E_r. Just downstream of the inlet where x/L < 1.0, no difference in E_r between the laminar and turbulent inflow case can be seen. However, at points further downstream, the E_r values for the turbulent inflow case become larger than that for the laminar inflow case; at the points further downstream (x/L > 8.0), the inlet turbulence effect is clearly confirmed. This is due to the fact that although small-scale turbulent eddies, which contained in the inflow turbulence, disappear, weak cross-sectional fluid motion still remains in the downstream region. This cross-sectional fluid motion is capable of disturbing the concentration boundary layer and promoting NO mixing, resulting in the increase of the reaction efficiency.

Particle Deposition Behavior

Particle deposition behaviour was investigated only in the turbulent inflow case. Figure 6 shows instantaneous distribution of particle positions. Particles which uniformly injected from the inlet move to the core region of the channel towards downstream. This is due to the fact that the flow from the wall to core region appears during the development of the wall boundary layer.

Figure 7 shows the streamwise distribution of particle deposition rate. Particle deposition rate takes a peak near the inlet and decreases towards downstream. Near the inlet, inner flow is turbulent, hence such disordered fluid motion frequently transports particles to the wall surface and enhance particle deposition. However, the inner flow transitions from turbulent to laminar flow and the fluid motion from the core region to wall disappears as flow

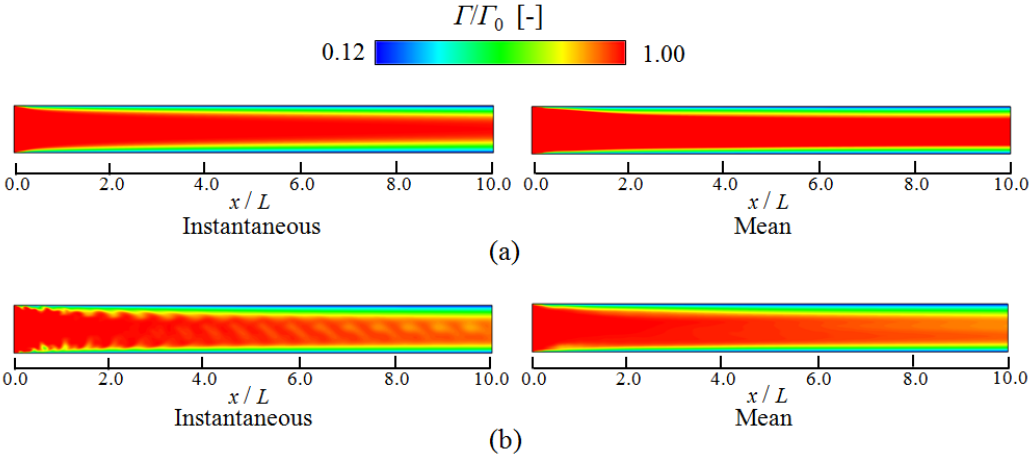

Figure 4. Instantaneous and time-averaged NO concentration on the plane of z=0: (a) laminar inflow case; (b) turbulent inflow case.

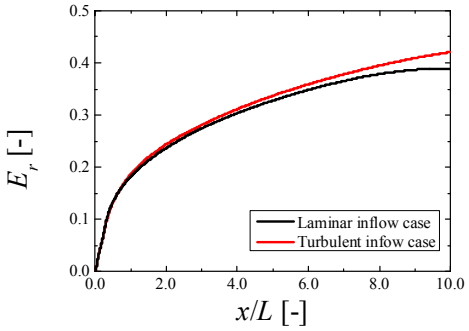

Figure 5. Streamwise distributions of reaction efficiency.

moves to the downstream, meaning the particles hardly reach wall and particle deposition is prevented. Consequently, the surface of monolith reactor is covered by particle only in the upstream region. Such result is also observed in the de-NO_x catalyst which is long-term used in the thermal power plant (Tanno, 2009)

CONCLUSION

Surface reaction behaviour occurred on the wall surface and particle deposition behaviour in the monolith reactor channel have been investigated performing a direct numerical simulation (DNS). The flow in a monolith reactor channel transitions from turbulent to laminar flow. Both surface reaction and particle deposition are promoted by turbulent eddies which exists in the upstream region. However, the region which exhibits the effect of turbulent eddies is different. For particle deposition, the effect of turbulent eddies is exhibits only in the upstream region, whereas such effect also exhibits in the downstream region for surface reaction. This is because of the remaining cross-sectional fluid motion caused by the inflow turbulence. Although the magnitude of the cross-sectional fluid motion is weak, such motion only affects gaseous flow and cannot affect heavy particle motion.

REFERENCES

Book, D.L., Boris, J.P. and Hain, K., 1975, "Flux-Corrected Transport. II: Generalizations of the Method", *Journal of Computational Physics*, Vol. 18 pp. 248–283.

Boris, J.P. and Book, D.L., 1973, :Flux-Corrected Transport. I. SHASTA, a Fluid Transport Algorithm that Works", *Journal of Computational Physics*, Vol. 11, pp. 38–69.

Boris, J.P. and Book, D.L., 1976, "Flux-Corrected Transport. III: Minimal-error FCT Algorithms", *Journal of Computational Physics*, Vol. 20 pp. 397– 431.

Beeckman, J.W and Hegedus, L.L., 1991 "Design of Monolith Catalysts for Power Plant NO_x Emission Control", *Industrial & Energy Chemistry Research*, Vol. 30, pp. 969-978.

Crowe, C. T., Sharma, M.P. and Stock, D.E., 1977, "The Particle Source-in Cell (PSI-Cell) method for Gas-Droplet Flows", *Trans. ASME I: J. Fluids Eng.*, Vol. 6, pp. 325-332.

Ferziger, J.H. and Peric, M., 2002, *Computational Methods for Fluid Dynamics*, third ed. Springer-Verlag.

Fogler, H. S., 2005, *Elements of Chemical Reaction Engineering*, Prentice-Hall PTR, Upper Saddle River, NJ, 2005.

Forzatti, P., 2001, "Present Status and Perspectives in De-NO_x SCR Catalysis", *Applied Catalysis A*, Vol. 222, pp. 221-236.

Glaze, D. J. and Frankel, S. H., 2000, "Effect of Dispersion Characteristics on Particle Temperature in an Idealized Nonpremixed Reacting Jet", *Int. J. Multiphase Flow*, Vol. 26, pp. 609-633.

Hays, R. E. and Kolaczkowski, S. T., 1994, "Mass and Heat Transfer Effects in Catalytic Monolithic Reactors", *Chemical Engineering Science*, Vol. 49, pp.3587-3599.

Huser, A. and Biringen, S., 1993, :Direct Numerical Simulation of Turbulent Flow in a Square Duct", *Journal of Fluid Mechanics*, Vol. 257, pp. 65-95.

Kim, J. and Moin, P., 1985, "Application of a Fractional-step Method to Incompressible Navier–Stokes Equations", *Journal of Computational Physics*, Vol. 59 pp. 308–323.

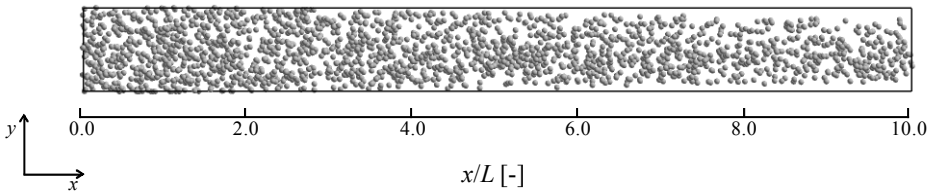

Figure 6. Instantaneous distribution of particle position.

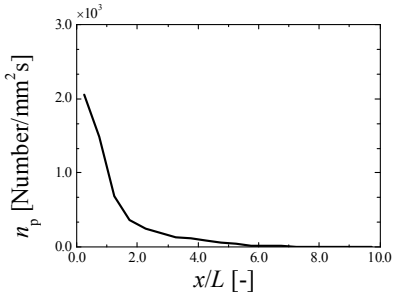

Figure 7. Streamwise distribution of particle deposition rate.

Michioka, T., 2001, *Development of Large Eddy Simulations of Turbulent Flows with a Chemical Reaction*, Ph.D. Thesis, Department of Mechanical Engineering, Kyoto University, (2001) (in Japanese).

Michioka, T., Sato, A. And Sada, K., 2003, "Large-eddy Simulation for the Tracer Gas Concentration Fluctuation in Atmospheric Boundary Layer, *Transactions of Japan Society of Mechanical Engineering Series B*, Vol. 69, pp. 868–875.

Phares D. J. and Sharma, G., 2006, "A DNS Study of Aerosol Deposition in a Turbulent Square Duct Flow", *Aerosol Science and Technology*, Vol. 40, pp. 1016-1024.

Roduit, B., Wokaum, A., and Baiker, A., 1998, "Global Kinetic Modeling of Reactions Occurring during Selective Catalytic Reduction of NO by NH_3 over Vanadia/Titania-Based Catalysts", *Industrial & Energy Chemistry Research*, Vol. 37, pp. 4577-4590.

Ström, H. And Sasic, S., 2012, "Heat and Mass Transfer in Automotive Catalysts –The Influence of Turbulent Velocity Fluctuation", *Chemical Engineering Science*, Vol. 83 pp. 128-137.

Tronconi, E. And Beretta, A., 1999, "The Role of Inter- and Intra-Phase Mass Transfer in the SCR-DeNO_x Reaction over Catalysts of Different Shapes", *Catalysis Today*, Vol. 52, pp. 249-258.

Williamson, J.H., 1980, "Low-Storage Runge-Kutta Schemes", *Journal of Computational Physics*, Vol. 35 pp. 48-56.

Winkler, C.M. and Rani, S.L., 2009, "Relative importance of the Lift Force on Heavy Particles due to Turbulence Driven Secondary Flows", *Powder Technology*, Vol. 190, pp. 310-318.